Modeling and Validation of Moving Coil Actuated Valve for Digital Displacement Machines

Nørgård, Christian; Bech, Michael Møller; Christensen, Jeppe Haals; Andersen, Torben O.

Published in:
I E E E Transactions on Industrial Electronics

DOI (link to publication from Publisher):
10.1109/TIE.2018.2808936

Publication date:
2018

Document Version
Accepted author manuscript, peer reviewed version

Modeling and Validation of Moving Coil Actuated Valve for Digital Displacement Machines

Christian Noergaard, Michael M. Bech, Jeppe H. Christensen, and Torben O. Andersen

***Abstract*—This paper concerns a novel moving coil actuator integrated with a high-performance seat valve for use in Digital Displacement Machines (DDM), which is an emerging fluid power technology that sets strict actuator requirements in order to get a high energy conversion efficiency. Hence, the mechanical switching time must be in the milli-second range and the actuator power consumption must be in range of few tens of watts. The objectives are two-fold: (i) to establish a proof-of-concept for the integrated actuator/valve that relies on several principles and mechanisms new or uncommon in fluid power applications and (ii) to formulate and validate a transient numerical model describing the actuator/valve. A coupled simulation model is established to predict the switching performance: transient electro-magnetic finite-element-analysis with dynamic re-meshing is coupled to a set of ordinary differential equations describing the motion dynamics. In this way, the movement induced hydro-mechanical fluid forces caused by rapid acceleration of the valve plunger is coupled with the electro-magnetic dynamics. The proposed model is compared rigorously against measurements obtained from a series of experiments based on a fully operational valve prototype. Comparisons of e.g. transient flux density, current, and plunger position show that the model describes both the actuator and the valve motion very well. Finally, results are presented when testing the prototype valve in fully operational DDM to establish proof-of-concept for the proposed valve concept. The actuator/valve is shown to be capable of rapid switching in less than 4 ms while only consuming approximately 45 W corresponding to 0.7% of the machine output power.**

***Index Terms*—Actuators, Mechatronics, Hydraulic Systems**

I. Introduction

DIGITAL Displacement (DD) Technology has the potential to improve the efficiency of variable displacement fluid power machinery, especially at partial displacements where conventional fluid power machines typically suffer from a poor efficiency [1], [2]. This, combined with the well known advantages of conventional fluid-power machines such as high power-density and good reliability and ruggedness, makes Digital Displacement Machines (DDMs) attractive candidates for several applications where fluid power previously have been unsuited. However, despite the potential of DD technology, a commercial breakthrough still awaits.

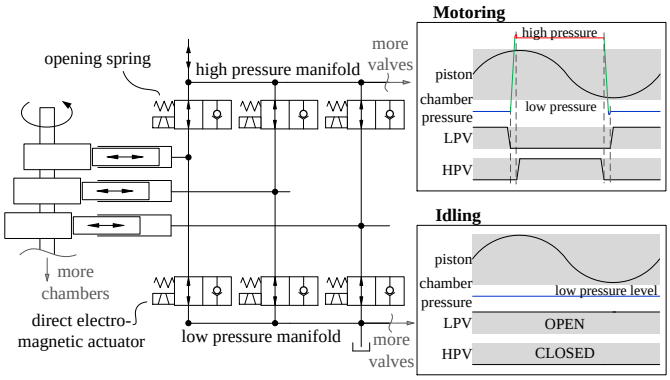

Fig. 1. (left): Sketch of a digital hydraulic fluid power pump/motor and (right) motoring- and idling operation cycles.

Fundamentally, in a DDM a number of cylinders are connected to a high and low pressure manifold through electrically controlled on/off switching valves. These valves are key components of the machine and they must ensure fast switching while imposing small electrical and flow power losses. Also, the valves must be robust to endure billions of cycles in applications such as e.g. hydro-static transmission systems in wind turbines [3]. Commercial valves meeting these requirements do not yet exist [4].

Fig. 1 illustrates the architecture of a DDM (*left*) and the so-called motoring and idling operation cycles (*right*). The valve symbols illustrate the functionalities of the valve concept presented in this paper i.e. a moving coil actuated normally open seat type check-valve. When operating in motoring mode oil is displaced from the high pressure to the low pressure manifold while doing work on the piston during the extending half of the stroke. In each cycle, one active closing and one passive opening occur for both the low pressure valve (LPV) and the high pressure valve (HPV). During the idling operation cycle, the LPV is kept open throughout the cycle, resulting in no work being done on the piston. The machine displacement is controlled by varying the fraction of motoring versus idling cylinders on a stroke-by-stroke basis. This enables rapid control of the total machine displacement. Importantly, a high efficiency can be maintained at low displacement ratios [4].

The fundamental ideas of the DD technology were conceived at the University of Edinburgh in the late 1980's

Manuscript received Octorber 12th, 2017; revised January 10th, 2018; accepted January 24th, 2018. This work was supported in part by the Department of Energy Technology at Aalborg University under Grant 130500038B awarded by Innovation Fund Denmark.

Christian Noergaard, Michael M. Bech, Jeppe H. Christensen and Torben O. Andersen are all with the Department of Energy Technology, Aalborg University, Alborg, Denmark (e-mail: {chn,mmb,jhc,toa}@et.aau.dk).

This article has been accepted for publication in a future issue of this journal, but has not been fully edited. Content may change prior to final publication. Citation information: DOI 10.1109/TIE.2018.2808936, IEEE Transactions on Industrial Electronics

which later resulted in the foundation of the company Artemis Intelligent Power (AIP). Over the years AIP has applied the technology to a wide range of applications including hybrid commercial vehicles [2], excavators [5], hybrid city buses [6] and also, in collaboration with Mitsubishi Heavy Industries, a 7 MW hydro-static wind-turbine transmissions system [7].

For DDMs having relatively large cylinders operating at high speed a new class of fast-switching valves is required which has a large flow capacity and a low pressure drop but still is capable of switching in the millisecond range. The state-of-the-art DDM's developed by AIP use solenoid actuators for switching of the seat/poppet valves, but concise valve performance information has not been published. In academia, solenoid [8], [9], moving coil [10] and moving magnet [11] actuated valves have previously been studied for DDMs.

Moving coil actuators are based on the Lorentz force principle [12]. A static flux generated by a permanent magnet exits leading to a superior transient force performance, compared against solenoids, because no delay is present between the coil current and the electro-magnetic force. Another advantage is that the force typically is almost position independent making valve design having large stroke lengths feasible. This is important for achieving large flow capacities. Also, a relatively long stroke length may reduce the axial flow forces induced on the moving member during flow conduction which in turn reduces the required actuator force [13]. Due to the superior transient performance and the linear force characteristics, moving coil actuators are typically used in applications such as audio speakers, camera lens positioning systems etc. Even though that the majority of valves used in fluid power systems are based on solenoid actuation principles commercial valves based on the moving coil principle are also available. For example, the Parker DF-Plus servo valve [14] exhibits promising transient performance. However, this particular valve is a spool type making it unsuited for high-efficient DD operation due to its leakage flow. In academia, moving coil based servo valves have been studied in [15], [16]: these are also spool based and aimed for much smaller flow capacities than needed for efficient high-speed DD operation. A generic disadvantage of the moving coil actuator is that a durable and flexible electrical connection is required to the moving coil. Depending on the application this may lead to more complicated designs consisting of many small parts.

To study the suitability and the potential of using moving coil based valves for DDM applications, a moving coil actuated seat valve have been developed by the authors. This paper focuses on modeling of the time-dependent switching behavior of the valve using a transient electro-magnetic finite-element-analysis coupled to a detailed lumped-parameter model of the motion dynamics. The correctness of the model is assessed by comparing simulation results against measured data obtained by a series of experiments on a prototype (PT) actuator/valve. Experimental results are presented with the PT valve deployed in a real DDM test-rig to establish a proof-of-concept under actual loading conditions.

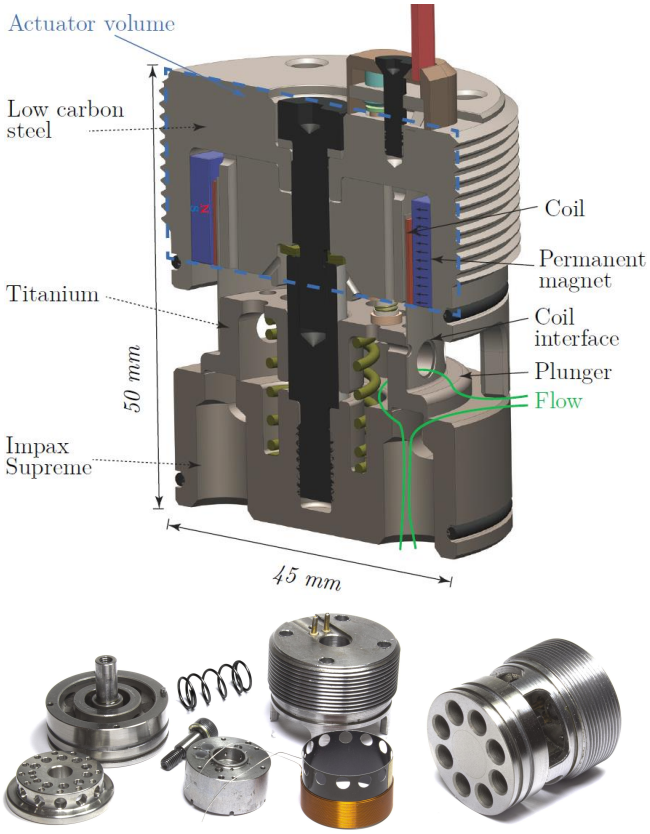

Fig. 2. Integrated moving coil acutator and seat valve design. (top) 3D sectional view and (bottom) the main parts of the realized prototype.

II. Moving Coil Actuated Seat Valve For DDMs

Figure 2 shows a sectional CAD model view (*top*) and the valve parts (*bottom*) for the developed PT. The valve of annular seat type has check-valve capability for flow entering from the bottom flow port. A spring is used to produce a passive opening force ensuring that the valve does not close due to axial flow forces during flow conduction. A slitted (to ensure galvanic insulation) titanium foil is glued to the plunger on which a coil is wound. The magnets are radially magnetized producing a close to uniformly distributed magnetic field perpendicular to the windings of the coil. The sintered neodymium shell magnets have a nickel-copper-nickel coating. The electrical interface between the moving coil and the stationary housing is based on spring connectors.

Because the coil is situated in the hydraulic oil it is exposed directly to the high cyclic pressures inherent of digital displacement operation. While imposing some additional mechanical stress, the oil serves well as electrical insulator and it effectively transports heat away from the coil through advection. The actuator core material is low carbon steel characterized by a relatively high magnetic saturation point. The plunger material is titanium due to its low weight and relatively high strength. The valve design was derived using multi-objective optimization to minimize the electrical and flow related losses when operating a 50 CC cylinder at 800 RPM leading to peak flow rates of 125 l/min, for detailed information see [17]. Table I list other key characteristics.

TABLE I
KEY CHARACTERISTICS FOR PROTOTYPE ACTUATOR/VALVE

Outer dimensions	Ø 45 mm x 50 mm
Maximum pressure	350 bar
Δp_{valve} @ ±120 l/min flow rate	+0.18/-0.48 bar [13]
Actuator principle	Moving coil
Actuator stroke length	2.5 mm
Rated supply voltage	48 V
Peak current	15 A
Valve closing time (approx.)	1.7-3.0 ms
Passive opening spring force	30-35 N
Moving mass	19 g
Number of coil turns	66

III. ACTUATOR/VALVE MODELING

The time-dependent behavior of the integrated acutator/valve assembly is modeled using a coupled model comprising transient electro-magnetic FEA and lumped models describing the electrical circuit and the valve movement. Figure 3 outlines the overall coupling between the submodels in COMSOL. The Electrical subsystem is implemented using the Electrical Circuit interface, the Mechanical subsystem is implemented using the ODE and DAE interface and the Electromagnetic subsystem is implemented using the geometry based Magnetic Fields interface.

A. Electro-magnetic FEA

The actuator is modeled in an axi-symmetric domain since the geometry is primarily rotational symmetric. The magnetic field is solved based on Maxwell equations using the magnetic vector potential approach. For the time-dependent case, the equations solved for each node of the solution domain are:

$$\sigma\frac{\delta \mathbf{A}}{\delta t} + \nabla \times \mathbf{H} = \mathbf{J}_{\text{e}} \qquad (1)$$
$$\mathbf{H} = f(\mathbf{B}) \quad \text{and} \quad \mathbf{B} = \nabla \times \mathbf{A},$$

where σ is the material conductivity, $\mathbf{A}$ the magnetic vector potential, $\mathbf{H}$ the magnetic field intensity, $\mathbf{B}$ the magnetic flux density and $\mathbf{J}_{\text{e}}$ the externally generated current density. The term $\sigma\frac{\delta \mathbf{A}}{\delta t}$ represents the currents induced in the material due to a time varying flux density (according to Faraday's law), often referred to as eddy currents.

Figure 4 illustrates the individual domains using a typical discretization. Further information about each of the numbered sub-domains is given Table II. Primary triangular mesh elements are used, except for regions being completely rectangular where quadrilateral elements are better suited. The zoom in Figure 4 shows the coil and permanent magnet region. Movement of the coil (to emulate valve closing) is accomplished by dynamically re-meshing regions 2 and 3 using the Deformed Geometry Interface in the multi-physics COMSOL software package. In the model, the plunger is not moved during simulation as it has negligible influence on the generated electro-magnetic force exerted on the moving valve member due to the low permeability of the plunger material.

The electrical and magnetic properties, needed to solve the magnetic diffusion equation (1), are also given in Table II. As

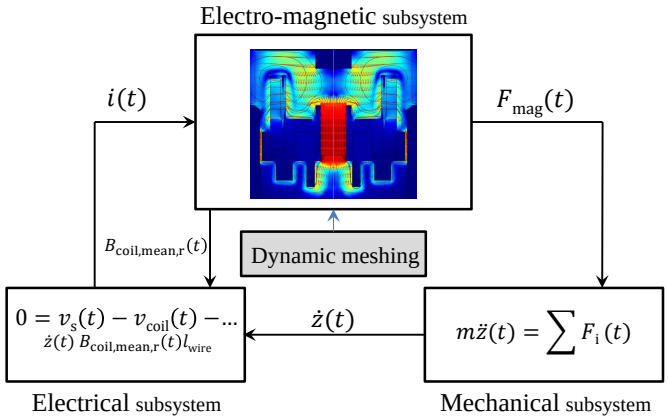

Fig. 3. Coupling between the electro-magnetic, electrical and mechanical subsystems that form the whole valve switching model.

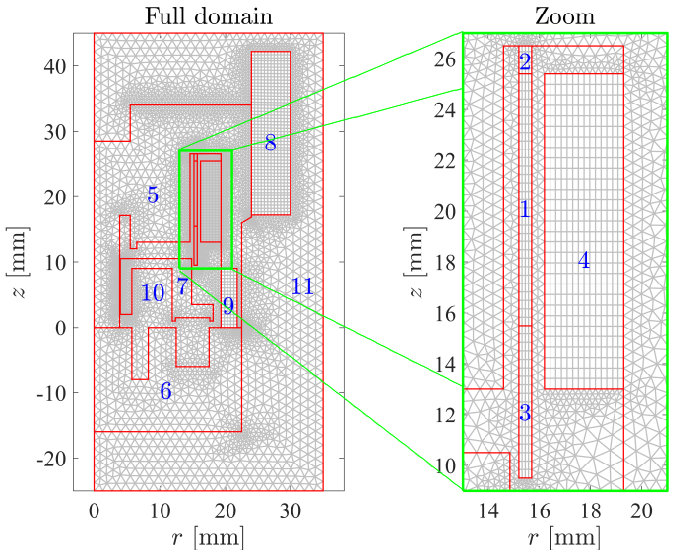

Fig. 4. FEA discretizaion. (left): full domain and (right): zoom in air gap.

TABLE II
INFORMATION FOR THE DOMAINS IN FIG. 4.

#	Material	σ [S/m]	μ_{r} [-]	Mesh Type
1	Copper	cf. (3)	1	Struct.
2	Air	0	1	Struct.
3	Air	0	1	Struct.
4	Sintered NdFeB	$2.14{\cdot}10^6$	1.045	Struct.
5	Automate steel	$6.29{\cdot}10^6$	cf. Fig. 5	Unstruct.
6	Impax Supreme	$6.29{\cdot}10^6$	cf. Fig. 5	Unstruct.
7	Titanium Grade 5	$2.60{\cdot}10^6$	1.0005	Unstruct.
8	Automate steel	$6.29{\cdot}10^6$	cf. Fig. 5	Struct.
9	Air	0	1	Struct.
10	Air	0	1	Unstruct.
11	Air	0	1	Unstruct.

can be seen, a constant permeability is used for air, copper, titanium and the permanent magnet. For the Automate steel and the Impax Supreme steel the BH-curves shown in Figure 5 are used to describe the constitutive relation between field intensity and flux density. The permanent magnet is modeled using:

$$\mathbf{B} = \mu_0(\mathbf{H} + \mathbf{M}), \qquad (2)$$

This article has been accepted for publication in a future issue of this journal, but has not been fully edited. Content may change prior to final publication. Citation information: DOI 10.1109/TIE.2018.2808936, IEEE Transactions on Industrial Electronics

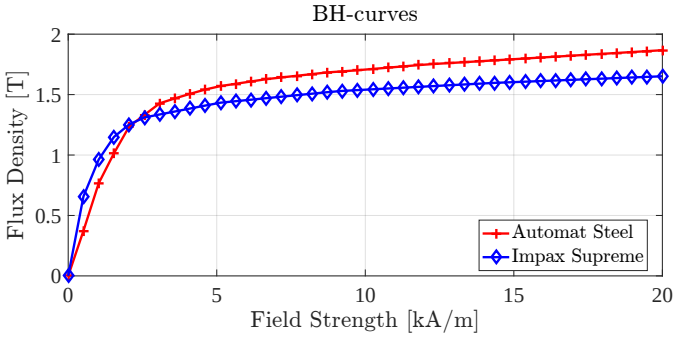

Fig. 5. BH-curves based on measurements [17] and material data sheet.

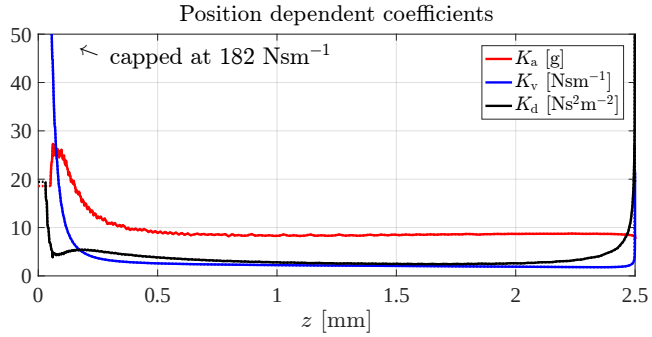

Fig. 6. Coefficients for the movement induced forces given in (8) [18].

where $\mathbf{M}$ is the magnetization. The material parameters are listed in Table II. The copper conductivity is temperature corrected as it has considerable influence on the coil resistance:

$$\rho_{\mathrm{cu}}(T) = \rho_{\mathrm{cu,T_0}}[1 + \alpha_{\mathrm{cu}}(T - T_0)], \tag{3}$$

where $\rho_{\mathrm{cu,T_0}}$ is the copper resistivity at the reference temperature T_0 being 20°C equal to $1.68{\cdot}10^{-8}\Omega$m, α_{cu} is the temperature coefficient of copper equal to 0.00404 K^{-1}. The outer boundary of the solution domain is modeled as a magnetic insulator condition that sets the tangential components of the magnetic potential to zero at the boundary.

B. Electrical Circuit Model

The coil voltage and current is modeled using a voltage source coupled to the distributed field model of the coil available in the Electrical Circuit physics package in COMSOL. COMSOL does not by default include the back-EMF term in the magnetic vector equation and instead it is included manually. The induced back-EMF voltage is dependent on the coil velocity, the coil geometry and the flux density normal to the current and movement direction. In total the voltage equation becomes

$$0 = v_{\mathrm{s}}(t) - \underbrace{i(t)Z_{\mathrm{coil}}(z,t)}_{v_{\mathrm{coil}}(t)} - \epsilon(\dot{z},t), \tag{4}$$

where $v_{\mathrm{s}}(t)$ is the voltage supplied by an external voltage source, $\epsilon(\dot{z},t)$ is the induced back-EMF voltage (not included in the magnetic diffusion equation in COMSOL) and Z_{coil} represents the voltage drop across the distributed field model of the coil. The back-EMF voltage ϵ is modeled as

$$\epsilon(\dot{z},t) = \underbrace{N\pi d_{\mathrm{coil}}}_{l_{\mathrm{wire}}} B_{\mathrm{coil,mean,r}}(t)\dot{z}(t), \tag{5}$$

where N is the number of turns, d_{coil} is the mean coil diameter and the axillary variable $B_{\mathrm{coil,mean,r}}(t)$ represents the mean radial flux density of the coil.

C. Mechanical Model

The model describing the motion of the moving valve member is

$$\begin{aligned} m\ddot{z} &= \sum F_{\mathrm{i}} \Downarrow \\ \ddot{z} &= \frac{1}{m}\left(F_{\mathrm{mov}}(z,\dot{z},\ddot{z}) + F_{\mathrm{mag}}(t) + F_{\mathrm{spring}}(z)\right), \end{aligned} \tag{6}$$

here, the spring force is modeled based on Hooks law:

$$F_{\mathrm{spring}} = (z_{\mathrm{pre}} - z(t))k_{\mathrm{spring}}, \tag{7}$$

where z_{pre} is the compression of the spring in the closed position and k_{spring} is the spring constant.

In (6) F_{mov} represents the movement induced forces acting on the plunger when being moved through the viscous oil:

$$F_{mov} = \underbrace{K_{\mathrm{a}}(z)\ddot{z}}_{\text{added mass term}} + \underbrace{K_{\mathrm{v}}(z)\dot{z}}_{\text{viscous term}} + \underbrace{K_{\mathrm{d}}(z)\,|\dot{z}|\,\dot{z}}_{\text{drag term}}, \tag{8}$$

where the position-dependent variables K_{a}, K_{v} and K_{d} shown in Figure 6 are based on a detailed CFD study and experiments of the movement-induced fluid forces performed for the plunger geometry published in [18].

By integration of acceleration (6), the velocity and position are obtained. The mechanical model is implemented using the ODE/ DAE interface in COMSOL. The mechanical end-stop at the closed position is modeled using a pseudo-model ensuring that the moving member is stopped when $z < 0$.

IV. Actuator/Valve Model Validation

Ultimately, the actuator/valve is installed in a DDM and under these operating conditions it is impossible to measure e.g. the displacement of the plunger or the flux density in the air gap. Therefore, a number of standalone tests are performed first where the valve is installed in specialized test rigs that allow to gather a variety of data. As detailed in the subsections below, a series of experiments are made to assess the validity of the model including measurements of:

- *A.* static radial flux density in the air gap,
- *B.* transient radial flux density in the air gap,
- *C.* static electro-magnetic actuator force as a function of current and plunger position,
- *D.* voltage, current and position during switchings.

A. Static Air Gap Flux Density

The air gap flux density is important to model accurately since the generated electro-magnetic force is proportional to the flux density, which was measured by fixing a Bell 5100 Series Gauss/Tesla Meter probe to the stationary part of a lathe while rotating the valve. Then, while turning the lathe and moving the probe in the air gap at low speed, continuous

This article has been accepted for publication in a future issue of this journal, but has not been fully edited. Content may change prior to final publication. Citation information: DOI 10.1109/TIE.2018.2808936, IEEE Transactions on Industrial Electronics

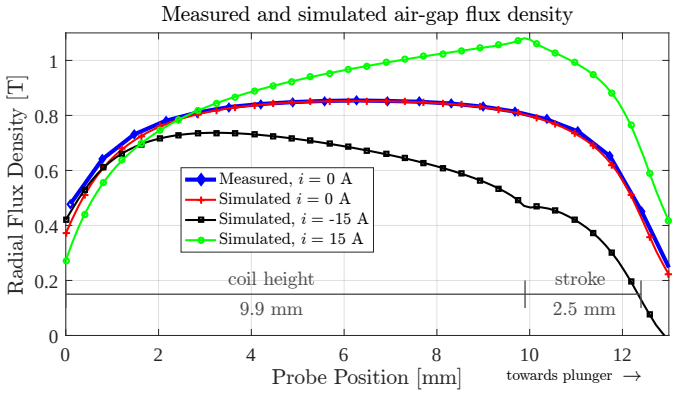

Fig. 7. Measured and calculated radial flux density in the air-gap.

measurements of the static axial flux density in the air-gap are obtained. The bottom part of the valve and the moving member, including the coil (see Fig. 2 and region 1, 6 and 7 of Fig. 4) was not installed during this experiment.

Post-processing the data leads to the average radial flux density shown in Fig. 7 for zero coil current, where the results predicted by the model also are included. Only small discrepancies are observed for $i = 0$. The simulated static flux density is also shown for coil currents of -15 A and 15 A to asses the sensitivity of air gap flux to the coil current. A negative current counteracts the flux generated by the magnet and produces force in the direction closing the valve. In the fully opened position the average flux density change is -17 % and 10 % for -15 A and 15 A, respectively.

B. Transient Air Gap Flux Density

The transient behavior of the magnetic flux density in the air-gap has also been measured when giving a voltage step to the actuator coil. Since this experiment is performed with the valve fully assembled, there is insufficient space for having the gauss meter probe in the air gap because it is occupied by the coil. Instead, a groove was made in one of the magnets making sufficient space for having the gauss meter probe next to the coil. A 30 V pulse with a duration of 10 ms was then given to the coil while measuring the radial flux density at the probe position. This was repeated while sweeping the position of the probe. In this way, the maps of the radial flux density $B_{\mathrm{r,gap}}(t, z_{\mathrm{probe}})$ in Fig. 8 were acquired. In this test, the moving member was fixed in the fully opened position. Due to the groove made in the permanent magnet to accommodate the probe, the static flux density has decreased significantly in the vicinity of the modified magnet. This can be observed by comparing the flux density in Fig. 8 before the voltage step is given with the static flux density in Fig. 7. However, the modification does not influence the time-dependent response of the magnetic field significantly since the permeability of air is close to that of the magnet.

To enable comparison with simulated results using the axi-symmetric model, the average static flux density is subtracted to get the radial flux density change:

$$\Delta B_{\mathrm{r,gap}}(t, z_{\mathrm{pr}}) = B_{\mathrm{r,gap}}(t, z_{\mathrm{pr}}) - B_{\mathrm{r,gap}}(-5\mathrm{ms}, z_{\mathrm{pr}}). \quad (9)$$

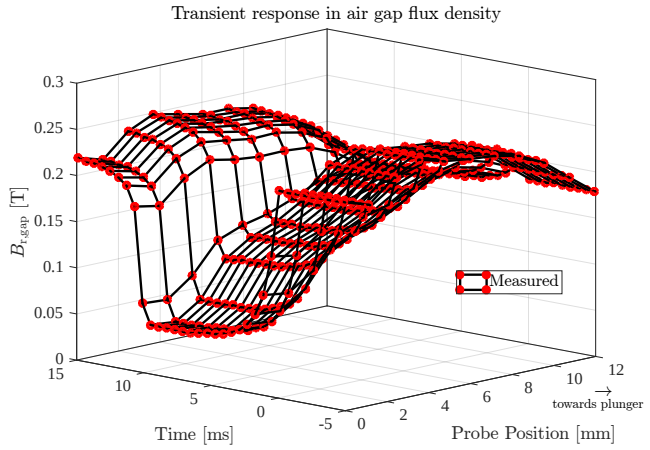

Fig. 8. Measurements of the transient radial magnetic flux density change in the air-gap when subjected to a voltage step of 30 V.

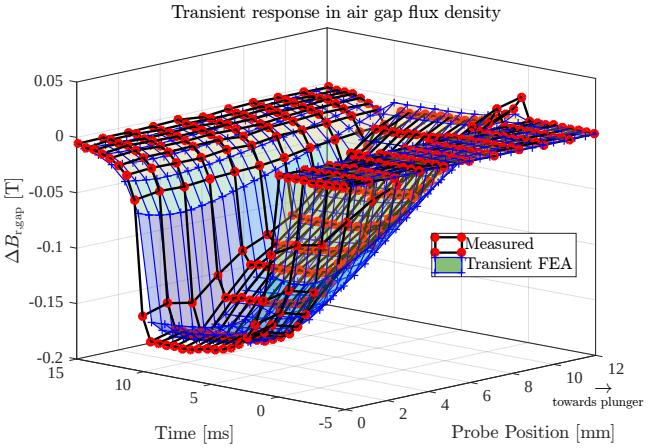

Fig. 9. Comparison of measurements and simulations of the transient radial magnetic flux density change in the air-gap during a voltage step of 30 V.

Fig. 9 compares (9) when using the measured flux map in Fig. 8 against corresponding simulated results. The temperature, used for calculation of the copper resistivity was set to 20°C. The comparison shows good coherence between measured and simulated results.

C. Static Actuator Force

The static actuator force has been measured as a function of coil current and plunger position. The actuator/valve assembly was mounted in fixture incorporated into a Sauter SD200N100 spring tester that locks the plunger in a certain position. A current pulse of sufficient width for steady state to occur-was applied and the resulting actuator force was recorded. Sweeping the position and the current amplitude allow the static actuator force to be mapped as shown in Fig. 10. Here, the corresponding simulations using the axi-symmetric model in a completely static case are also included. Again, a temperature of 20°C was used. The measured and simulated results primarily show good correspondence, although at the extreme positions notable discrepancies are present, especially

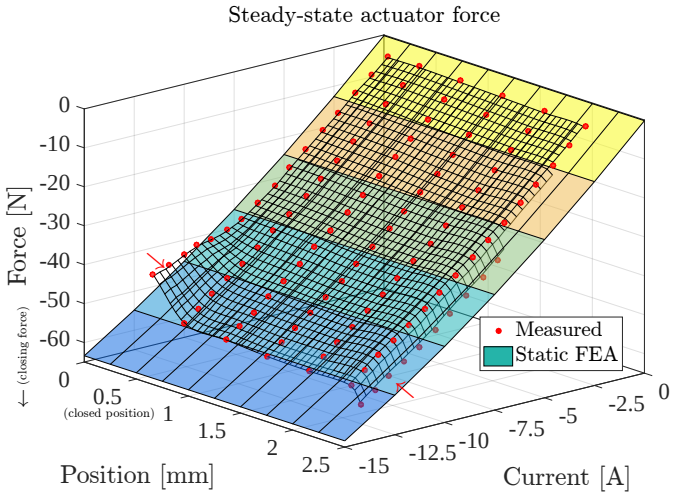

Fig. 10. Measured and simulated static actuator force vs. current and position.

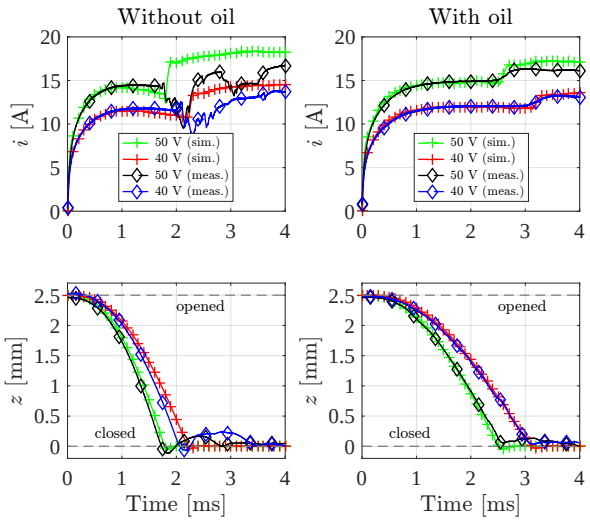

Fig. 11. Measured and simulated switching performance. (left): in air (right): submerged in hydraulic oil.

at larger (absolute) currents as indicated by the red arrows in the figure. These errors are due to limitations of the test setup and do not represent the actual generated actuator force.

D. Valve Switching Performance

The position, the voltage and current of the actuator have been measured on an 12 bit oscilloscope during switchings. A Keyence LK-G82 laser displacement sensor was used for position measurement. The tests have been conducted with the valve situated in air, and with the valve completely submerged in hydraulic oil. Measured results are shown for voltage steps of approximately 30 V and 50 V amplitude in Fig. 11 together with the corresponding simulation results using the model described earlier. Considering the case without oil in Fig. 11, the measured results shows that the valve closes in approximately 1.7 ms and 2.7 ms for the 50 V and 30 V cases, respectively. At the instants of the valve closing, the coil current drops rapidly. This is caused by the spring connector used for the electrical interface between the moving coil and the stationary housing. However, when the actuator/valve operates is in oil, a smooth increase in the current is observed as expected due to the back-EMF voltage going to zero. In oil, the valve closing time is measured to be approximately 2.5 ms @ 50 V and 4.2 ms @ 30 V voltage step.

The simulated results have been performed by supplying the measured voltage waveforms as input to the model. For the oil case, the full mechanical model is used with the coefficients shown in Figure 6 and for the case without oil the movement induced force F_{mov} is set to zero. The temperature used for the copper resistance was for the no oil case 45°C and for the oil case 65° C, corresponding to coil resistances of 2.38 and 2.54 Ω respectively. Good correspondence is seen for all the presented results proving the that presented model is capable of predicting the transient behavior of the valve quite well. Notable deviation is present for the simulated current after the valve is closed for the 50 V cases. This is expected to be because the wire resistance increases slight during the closing. In the simulations, a mesh consisting of approximately 6000 elements was used and a variable time-step solver was employed with step sizes typically ranging between $1{\cdot}10^{-9}$ ms and the maximum allowed step-size $20{\cdot}10^{-6}$ ms. The model evaluation time is less than 10 minutes using an Intel i7 2.8 GHz processor with 16 GB memory.

V. Valve Test in Digital Displacement Machine

To establish proof-of-concept for the proposed switching valve concept tests have been performed with the prototype actuator/valve deployed in a inhouse-built DDM test rig. Below, the DDM test rig is presented and experimental results are presented for both motoring and pumping operation cycles.

A. DDM Test Rig

A DDM test rig has been built with the main objective to perform in-situ testing of fast switching valves [19]. A commercial radial piston machine has been modified by blocking the connection between the port plate and one out of five machine cylinders. A customized manifold was attached to a modified cylinder head in order to access the pressure chamber. The manifold connects the piston chamber to the high and low pressure oil supply by means of two prototype valves and in this way a one-cylinder version of Figure 1 was realized. Each cylinder of the machine has a displacement of 50 CC/rev leading to peak valve flows of 125 l/min during the maximum tested speed (800 RPM).

A photo of the experimental setup and the overall layout of the hydraulic circuit are shown in Figures 12 and 13, respectively. Accumulators are used both at the low and high pressure port of the LPV and HPV respectively to stabilize the pressures p_{L} and p_{H}. The pressure reducing valve (2) in Figure 13 is used to control the pressure level. In case of pumping operation the directional valve (1) is set as drawn, the gate valve (4) is closed and the pressure relief valve (3) is used to set the desired pressure level and to dissipate the fluid power through throttling. In case of motoring, the gate valve (4) is open and the directional valve (1) is switched

This article has been accepted for publication in a future issue of this journal, but has not been fully edited. Content may change prior to final publication. Citation information: DOI 10.1109/TIE.2018.2808936, IEEE Transactions on Industrial Electronics

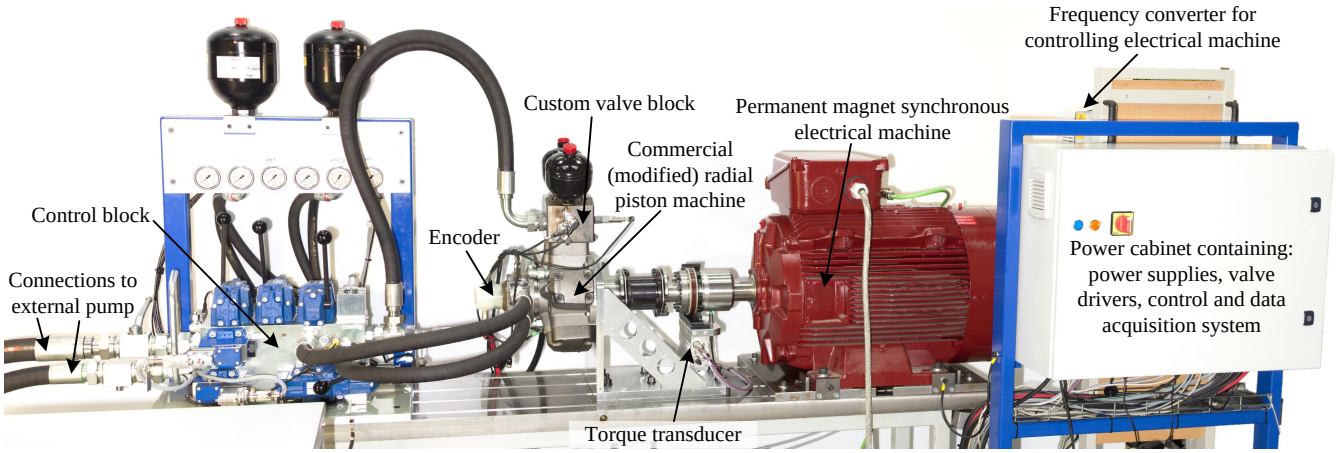

Fig. 12. Photo of test rig for testing of valves in digital displacement operation in both motoring and pumping operation.

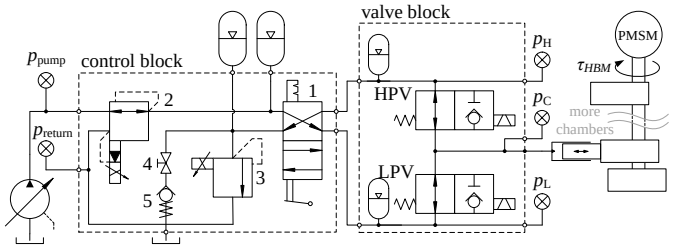

Fig. 13. Simplified schematic of the hydraulic circuit layout.

to the other state. During tests, the remaining four cylinders are effectively disabled by short circuiting the machine ports (another accumulator, not shown on the schematic, is used to stabilize this pressure string).

The shaft of the radial piston machine is connected to a 85 kW three-phase permanent magnet synchronous machine (PMSM) (model: Leroy Somer LSRPM250ME-T). The PMSM is speed controlled using a high-performance four quadrant drive which has a bi-directional mains interface. The actuators are controlled using in-house designed and built driver electronics. The test rig is well-equipped with sensors for measurement of e.g. pressure dynamics, shaft position and torque. The whole system is controlled by a fully customized National Instruments hardware platform using a mix of FPGA functionality and real-time processors.

For the test presented in the following subsection, the moving coil actuated prototype valve is installed as the LPV. Another prototype valve [11] based on the moving magnet actuator principle is used for the HPV.

B. DDM Test Results

Fig. 14 shows an DD motoring operation cycle at approximately 100 bar machine pressure span and 800 RPM. As the piston approaches the top dead center (TDC), the closing signal is given to the LPV. Approximately 3.0 ms later, the valve impacts with the end stop at the closed position. At this instant the current i_{L} increases rapidly because the back-EMF goes to zero. After the LPV valve is closed, the chamber pressure increases rapidly until reaching the high-pressure supply level where the HPV valve passively opens due to the check valve functionality. As the piston approaches the bottom dead center (BDC), the HPV valve is actively closed and then the chamber decompresses. When reaching the low-pressure supply level, the LPV valve opens passively. When an actuator is not energized, the open circuit voltage is measured. In this way, the passive opening of the LPV can be monitored based on the induced back-EMF voltage. The valve opening time is estimated to 3.3 ms in this way. The simulated position and current of the LPV are obtained using described model with the measured voltage as input. The simulated current corresponds well with the measured.

The instantaneous power delivered to the shaft is

$$p_{\mathrm{shaft}}(t) = p_{\mathrm{c}} \frac{V_{\mathrm{d}}}{2} \dot{\theta} \sin(\theta), \tag{10}$$

where V_{d} is the cylinder displacement, p_{c} is the measured chamber pressure and θ is the shaft angle relative to the TDC. Calculating the average of (10) across one revolution cycle gives an average shaft power of 6.21 kW. The average electrical power consumed by the LPV moving coil actuator is 44.5 W corresponding to 0.72 % of average shaft power.

Figure 15 illustrates the performance during a DD pumping operation cycle at 800 RPM and approximately 100 bar. During pumping, the LPV is closed at or shortly after the BDC. Again, the LPV closing time is deducted from the current waveform to be approximately 3.0 ms. After the LPV is closed, the chamber compresses and the HPV subsequently opens passively. Oil is displaced to the high-pressure manifold as the piston moves towards the TDC, where the HPV valve is closed after which the chamber decompresses and the LPV valve opens passively. Again the simulated current is observed to correspond well with the measured. Based on the induced back-EMF voltage the LPV opening time is estimated to be 2.2 ms. The faster opening occurs since the valve opening is carried out further from the respective dead center. Using (10), the average mechanical input power is calculated to be -6.23 W. The average electrical power consumed by the LPV is 44.7 W corresponding to 0.72 % of the average input power. The results shown in Figure 14 and 15 were sampled with the oil temperature ranging between 40°C and 50°C.

This article has been accepted for publication in a future issue of this journal, but has not been fully edited. Content may change prior to final publication. Citation information: DOI 10.1109/TIE.2018.2808936, IEEE Transactions on Industrial Electronics

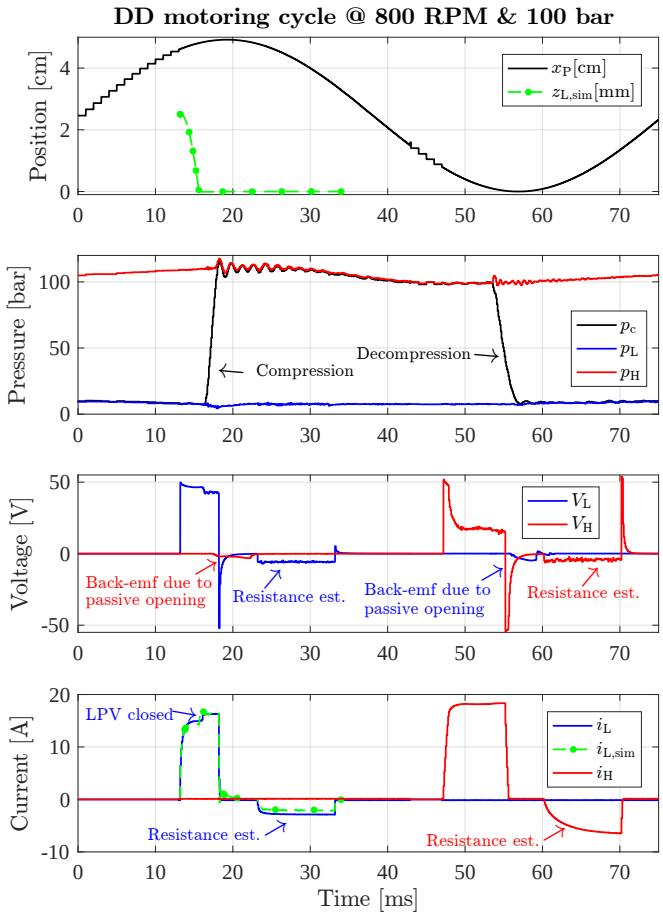

Fig. 14. DDM motoring: experimental results at 800 RPM and 100 bar.

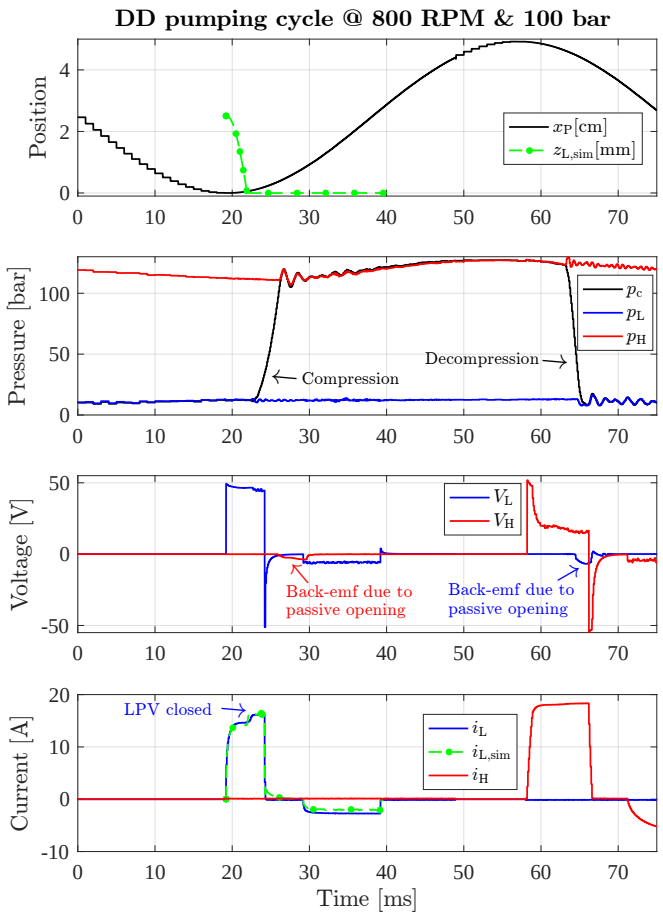

Fig. 15. DDM pumping: experimental results at 800 RPM and 100 bar.

VI. Conclusion

The work presented in this paper has demonstrated that a moving coil actuated switching valve can be deployed in digital displacement fluid power machines operating at relatively high speed. Indeed the use of a moving coil actuator in such an application is quite untraditional and unproven but nevertheless the experimental work reported in this paper illustrates that such a concept may be realized. Furthermore, the presented actuator/valve performs very well: the valve switching speed is typically less than 4 ms and the power needed to drive the actuator is in the range of a 25-50 watts and combined with the low pressure drop versus flow the overall performance in DDM operation is good.

In order to refine the design of the next generation of the actuator/valve even further, another objective of the reported work is to validate detailed numerical models of a valve actuated by a moving coil principle. The developed model couples transient 2D electro-magnetic finite element analysis with a lumped model of the electric circuit driving the coil and with a lumped model describing the plunger motion dynamics that takes movement-induced fluid forces into account. Based on a series of measurements on an actuator/valve prototype, it is concluded that switching characteristics predicted by the model accurately represents the actual switching performance. Also, special setups and techniques were used to measure the air gap flux density both during steady state and transient operation. Comparisons with results produced by the model shows good correspondence. Finally, the static force versus current and position was measured and the results shows that the model also predicts the electro-magnetic force accurately.

References

[1] K. J. Merrill, M. A. Holland, and J. Lumkes, Jr., "Efficiency analysis of a digital pump/motor as compared to a valve plate design," in *Proc. of the 7th International Fluid Power Conference*, Aachen, Germany, 2010.

[2] J. Taylor, W. Rampen, A. Robertson, and N. Caldwell, "Digital displacement hydraulic hybrids - parallel hybrid drives for commercial vehicles," Artemis Intelligent Power, Ltd., Paper presented at the annual JSAE congress, Kyoto, Japan, Tech. Rep., 2011.

[3] M. Umaya, T. Noguchi, M. Uchida, M. Shibata, Y. Kawai, and R. Notomi, "Wind power generation - development status of offshore wind turbines," Mitsubishi Heavy Industries, Technical Review, 2013, vol. 50, no. 3.

[4] D. B. Roemer, "Design and optimization of fast switching valves for large scale digital hydraulic motors," Ph.D. dissertation, Department of Energy Technology, Aalborg University, 2014.

[5] Artemis Intelligent Power, Ltd., "Digital displacement hybrid excavator - update," 2016, url:www.artemisip.com/digital-displacement-hybrid-excavator, accessed 2017-08-31.

[6] J. Taylor, W. Rampen, D. Abrahams, and A. Latham, "Demonstration of a digital displacement hydraulic hybrid - a globally affordable way of saving fuel," in *Proc. of the Annual JSAE Congress*, Pacifico Yokohama, Japan, 2015.

[7] M. Foster, "World's largest floating turbine installed at Fukushima," Wind Power Offshore, Jan. 2015, url:www.windpoweroffshore.com/article/1358221/worlds-largest-floating-turbine-installed-fukushima, accessed 2017-08-31.

[8] D. B. Roemer, P. Johansen, H. C. Pedersen, and T. O. Andersen, "Design and modelling of fast switching efficient seat valves for digital displacement pumps," *Transactions of the Canadian Society for Mechanical Engineering*, vol. 37, no. 1, pp. 71–88, 11 2013.

[9] J. Mahrenholz and J. Lumkes, Jr., "Analytical coupled modeling and model validation of hydraulic on/off valves," *Journal of Dynamic Systems, Measurement, and Control*, vol. 132, DOI 10.1115/1.4000072, pp. 1–10, Jan. 2010.

[10] D. Roemer, P. Johansen, M. Bech, and H. Pedersen, *Simulation and Experimental Testing of an Actuator for a Fast Switching On-Off Valve Suitable to Efficient Displacement Machines*. Japan Fluid Power System Society, 2014.

[11] E. L. Madsen, J. M. Joergensen, C. Noergaard, and M. M. Bech, "Design optimization of moving magnet actuated valves for digital displacement machines," in *Proc. of the ASME/Bath Symposium on Fluid Power and Motion Control, Sarasota, FL, US*. American Society of Mechanical Engineers, 2017.

[12] J. R. Brauer, *Magnetic actuators and sensors*. John Wiley and Sons, 2006.

[13] C. Noergaard, M. M. Bech, J. H. Christensen, and T. O. Andersen, "Flow characteristics and sizing of annular seat valves for digital displacement machines," *Modeling, Identification and Control*, p. ?, 2017.

[14] Parker Hannifin Corporation, "Direct operated proportional dc valves series d1fp," Data sheet.

[15] B. J. Sung, "Design of voice coil type linear actuator for hydraulic servo valve operation," *American Journal of Electrical Power and Energy Systems*, vol. 4, DOI 10.11648/j.epes.s.2015040501.11, no. 5-1, pp. 1–8, 2006.

[16] L. Nascutiu, "Voice coil actuator for hydraulic servo valves with high transient performances," in *2006 IEEE International Conference on Automation, Quality and Testing, Robotics*, vol. 1, DOI 10.1109/AQTR.2006.254522, pp. 185–190, May. 2006.

[17] C. Noergaard, M. M. Bech, D. B. Roemer, and H. C. Pedersen, "Optimisation of moving coil actuators for digital hydraulic machines," in *Proc. of the* 8^{th} *Workshop on Digital Fluid Power*, pp. 39–54, Tampere, Finland, May. 2016.

[18] N. C. Bender, C. Noergaard, and H. C. Pedersen, "Experimental validation of flow force models for fast switching valves," in *Proc. of the ASME/Bath Symposium on Fluid Power and Motion Control*. Sarasota, FL: American Society of Mechanical Engineers, 2017.

[19] C. Noergaard, J. H. Christensen, M. M. Bech, A. H. Hansen, and T. O. Andersen, "Test rig for valves of digital displacement machines," in *Proc. of the Ninth workshop on digital fluid power*, Aalborg, Denmark, 2017.

Christian Noergaard was born in 1986. He received his M. Sc. in Mechatronic Control Engineering from the department of Energy Technology, Aalborg University, 2014. Ever since he has been working towards achieving the Ph.D. degree in optimization and design of fast switching active check valves for digital displacement machines with the same department.

Michael M. Bech was born in 1971. He received the M.Sc. and Ph.D. degrees in power electronics in 1990 and 1995, respectively, from Aalborg University Denmark. He has been associate professor at the Department of Energy Technology at the same university since 2002 except for the period 2006-2009, where he was a senior engineer at Motorola Mobile Devices. His main research interests include a broad range of disciplines ranging from power electronics and their applications to optimal design and control of mechatronic components and systems.

Jeppe H. Christensen was born in 1989. He received his M. Sc. in Electro Mechanical System Engineering from the department of Energy Technology, Aalborg University, 2015. Ever since he has been employedas a research assistent with said department to assist with experimental research in Digital Displacement technology.

Torben O. Andersen was born in 1966. He received the B.Sc. M.E. degree from the University of Southern Denmark, Odense, Denmark, in 1989, and the M.Sc. and Ph.D. degrees in mechanical/control engineering from the Technical University of Denmark, Lyngby, Denmark, in 1993 and 1996, respectively. From 1996 to 2000, he was with the R&D Department, Sauer-Danfoss A/S, where he worked in the area of fluid power and control engineering. In 2000, he joined Aalborg University, Aalborg, Denmark, as an associate professor. Since 2005, he has been a Full Professor in fluid power and mechatronics. His main research interests include design and control of mechatronic systems.